The Astrophysical Journal, 681: L37–L40, 2008 July 1

THE SOLAR MAGNETIC FIELD AND CORONAL DYNAMICS OF THE ERUPTION ON 2007 MAY 19

Y. Li,[1] B. J. Lynch,[1] G. Stenborg,[2] J. G. Luhmann,[1] K. E. J. Huttunen,[1,3]
B. T. Welsch,[1] P. C. Liewer,[4] and A. Vourlidas[5]

Received 2008 February 1; accepted 2008 May 23; published 2008 June 11

ABSTRACT

The solar eruption on 2007 May 19, from AR 10956 near solar disk center, consisted of a B9.5 flare (12:48 UT), a filament eruption, an EUV dimming, a coronal wave, and a multifront CME. The eruption was observed by the twin *STEREO* spacecraft at a separation angle of 8.5°. We report analysis of the source region photospheric magnetic field and its preeruption evolution using MDI magnetograms, the coronal magnetic field topology estimated via PFSS modeling, and the coronal dynamics of the eruption through *STEREO* EUVI wavelet-enhanced anaglyph movies. Despite its moderate magnitude and size, AR 10956 was a complex and highly nonpotential active region with a multipolar configuration, and hosted frequent flares, multiple filament eruptions, and CMEs. In the 2 days prior to the May 19 eruption, the total unsigned magnetic flux of the region decreased by ~17%. We interpret the photospheric magnetic field evolution, the coronal field topology, and the observed coronal dynamics in the context of current models of CME initiation and discuss the prospects for future MHD modeling inspired by these analyses.

Subject headings: Sun: corona — Sun: coronal mass ejections (CMEs) — Sun: filaments — Sun: flares — Sun: magnetic fields

Online material: mpeg animations

1. INTRODUCTION AND EVENT OVERVIEW

One of the primary goals of the *STEREO* mission is to study the 3D structure of coronal mass ejections (CMEs) and their eruption processes (Howard et al. 2007). Special interest arises for 2007 May 19 CME from AR 10956 near solar disk center when the *STEREO* twin spacecraft were at a separation angle of 8.5°, well within the optimal range for 3D viewing and reconstruction of the corona using multiwavelength SECCHI observations (Liewer et al. 2008 and references therein). The CME on May 19 was the most likely eruption associated with the interplanetary CME (ICME) observed May 21–22 by *STEREO A* and *B*, *ACE*, and *Wind* (Huttunen et al. 2008). Complimentary solar observations are available from the *SOHO* and *Hinode* spacecraft and the BBSO Hα network. This event provides the first opportunity to study the 3D evolution and dynamics of a solar eruption, from its preeruptive configuration through the CME initiation and filament eruption to multipoint in situ observations of the ejecta. In this Letter we analyze the photospheric and coronal magnetic field configuration and evolution together with the 3D view of the coronal dynamics in order to discriminate between CME initiation mechanisms (Antiochos et al. 1999; Linker et al. 2001; Li & Luhmann 2006).

AR 10956, located at ~3° north and ~1° west of the central meridian at the eruption time, was the main source of activity of the solar minimum Sun. Despite its moderate magnitude and size, AR 10965 had a complex magnetic configuration with multiple neutral lines (see § 2 for details) and a highly nonpotential coronal structure. The region generated frequent flares (22B and 2C; *GOES*), multiple filament eruptions, and CMEs.[6] Multiwavelength observations of the preeruption Sun on May 19 are shown in Figure 1. The erupting filament to the north of the active region is best seen in the Hα image (*left panel*). SECCHI EUVI has observations in four wavelengths (Wusler et al. 2004) with the EUV 171 Å image presented in the center panel, and three wavelet-enhanced EUVI anaglyph movies are attached. The right panel is a *Hinode* XRT soft X-ray image showing two bright sigmoids that appear to colocate with two of the magnetic neutral lines. In the EUV and soft X-ray images, two low-latitude coronal holes on the southern hemisphere, east and west of the active region, are the sources of the high-speed solar wind streams leading and trailing the ICME (Huttunen et al. 2008).

The May 19 B9.5 flare (began at 12:48 UT and peaked at 13:02 UT; *GOES*) was accompanied by the filament eruption, posteruption flare loops, EUV dimming (reaching maximum spatial extent at 13:12 UT), a coronal EUV wave, and a faint, multifront CME in coronagraph images (LASCO and SECCHI). The most rapidly expanding feature in white-light images following the flare and filament eruption had a plane-of-sky speed of 958 km s^{-1}.

2. MAGNETIC FIELD EVOLUTION AND TOPOLOGY

The evolution of the AR photospheric magnetic fields are analyzed utilizing the 96 minute cadence of the MDI line-of-sight magnetograms. In the left panel of Figure 2, the magnetic distribution at 12:47 UT is shown in a full-disk magnetogram, where the positive (negative) polarity is white (black). The center panel shows a zoomed-in view of the AR at original MDI resolution (Scherrer et al. 1995). The right panel shows a smoothed version overplotted with white (black) dashed lines

[1] Space Sciences Laboratory, University of California, Berkeley, CA 94720; yanli@ssl.berkeley.edu, blynch@ssl.berkeley.edu, jgluhman@ssl.berkeley.edu, huttunen@ssl.berkeley.edu, welsch@ssl.berkeley.edu.

[2] Interferometrics, Inc., 13454 Sunrise Valley Drive, Herndon, VA 20171; stenborg@kreutz.nascom.nasa.gov.

[3] Department of Physical Sciences, Theoretical Physics Division, University of Helsinki, Finland.

[4] Jet Propulsion Laboratory, California Institute of Technology, Pasadena, CA 91109; paulett.liewer@jpl.nasa.gov.

[5] Space Science Division, Naval Research Laboratory, Washington, DC 20375; vourlidas@nrl.navy.mil.

[6] See images and movies at http://stereo-ssc.nascom.nasa.gov/browse/2007/05/19/index.shtml.

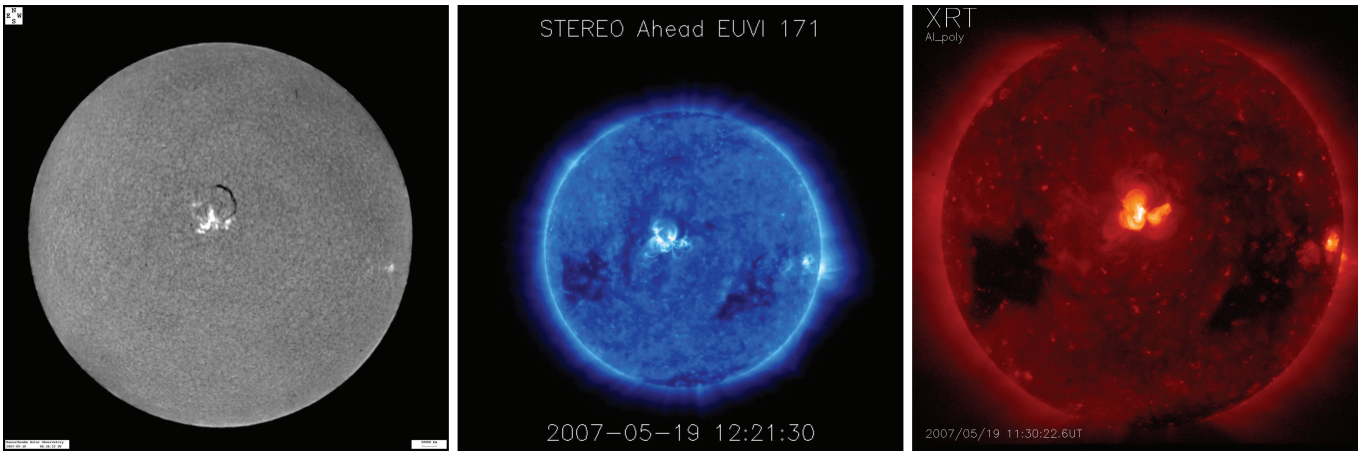

FIG. 1.—Multiwavelength solar images of the preeruption Sun on 2007 May 19. *Left*: BBSO global network Hα image (Kanzelhoehe) at 6:36 UT. *Middle*: SECCHI EUVI 171 Å image at ~12:21 UT. *Right*: *Hinode* XRT image at 11:30 UT. [*Wavelet-enhanced EUVI anaglyph movies at 171 Å, 195 Å, and 304 Å are available in the electronic edition of the Journal.*]

denoting negative (positive) contours. The solid white lines indicate the neutral lines (NLs). The time evolution of the original and smoothed magnetogram data can be seen in the attached movies. The magnetic field of the AR has a multipolar configuration with multiple photospheric magnetic NLs, marked as west (WNL), central (CNL), and east (ENL). Although there are small perturbations as a result of the overall diffusion of magnetic flux elements, in the strong-field regions, the NLs are well defined and remain approximately stationary in the period leading up to the eruption. The erupting filament was located in the weak-field region north of the AR (see § 3), where the photospheric NL is less well defined and highly variable with time.

We measured the magnetic flux in each frame of the zoomed-in magnetogram at original resolution, when the center of the active region was within 30° of the central meridian. Figure 3 gives the evolution of the sum of unsigned magnetic flux (*black solid line*), positive flux (*blue dot-dashed line*), and negative flux (*red dotted line*) from May 17 to 21, and the onset time of the flare (*black dashed line*). The total unsigned magnetic flux decreased by ~17% during the 2 days prior to the eruption. Interestingly, the positive and negative polarities behave differently. The positive flux decreased at a lower rate of ~14%, and the negative flux at a higher rate of ~20% in the 2 days preeruption. After the eruption, positive flux began to increase while the negative flux continued to decrease, resulting in the leveling of the unsigned flux. Clear flux cancellation and field reduction were taking place at the CNL and to a lesser extent at the WNL (see Fig. 2, *right*). The WNL is the 2007 May 19 flare site and the location of the southern end of the erupting filament. It has been proposed that flux cancellation/reduction increases the relative magnetic free energy of the system and could be the initiation mechanism responsible for some CMEs (Linker et al. 2001; Welsch 2006).

The coronal magnetic fields are estimated using the PFSS model approximation (e.g., Luhmann et al. 1998) based on the daily updated MDI synoptic map for May 19. Figure 4*a* shows the global coronal magnetic structure of the helmet streamer belt (*yellow field lines*). Even though shown during solar minimum, the streamer belt is highly inclined over the active region. The PFSS streamer belt structure compares favorably with coronagraph images (see footnote 6). The low-latitude coronal holes, defined by the helmet streamer boundaries flanking the AR, are in good agreement with the EUVI and XRT observations of Figure 1. Figure 4*b* shows representative PFSS coronal magnetic field lines originating from AR 10956 and the overlying flux system. The field lines of the multiflux system are color coded by their connectivity as dark blue, green, and

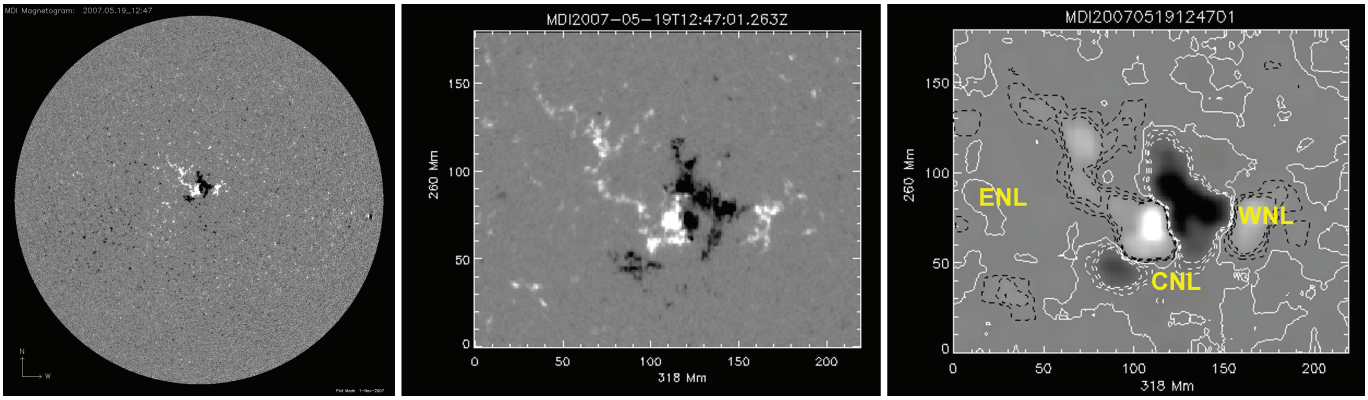

FIG. 2.—*Left*: MDI magnetogram at 12:47 UT on 2007 May 19; positive (negative) polarity in white (black). *Middle*: Zoomed-in magnetogram centered on AR 10956. The maximum field strength in this frame is ~1200 G. *Right*: Smoothed magnetogram with contours. The solid white lines are magnetic NLs and the dashed black (white) lines are positive (negative) contours. WNL = west neutral line; CNL = central neutral line; ENL = east neutral line. [*The middle and right panels are available as mpeg animations in the electronic edition of the Journal.*]

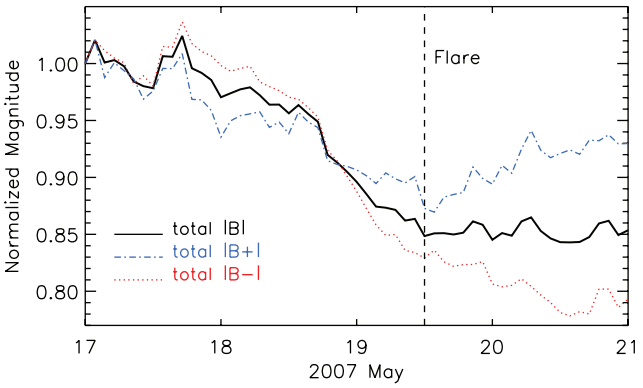

FIG. 3.—Magnetic flux evolution of the zoomed-in magnetogram (Fig. 2, *middle*) from 2007 May 17 to 21. The vertical black dashed line marks the onset of the flare. The solid black line represents the sum of the unsigned magnetic flux; the blue dot-dashed line shows the sum of positive flux and the red dotted line shows the sum of negative flux. The total unsigned flux shows a decrease of ~17% in the two days before eruption.

light blue for the ENL, CNL, and WNLs in Figure 2, respectively. The topological boundary (separator surface) between flux systems is indicated by a pair of purple field lines. The multiflux topology may correspond to a lateral magnetic breakout eruption, where reconnection at the coronal null point between the two side lobes (*dark blue and light blue*) transfers the restraining flux (*light blue*) overlying the filament to the central (*green*) and streamer (*yellow*) flux systems. This lateral reconnection reduces the restraining force on the filament, thus leading to a runaway destabilization of the system (Aulanier et al. 2000; Williams et al. 2005).

Figure 4*c* shows a zoomed-in view of the Hα filament overlaid with tie points (marked as crosses) of the filament in EUVI *A* and *B* 304 Å images used in Liewer et al. (2008) for 3D reconstruction. Figure 4*d* shows the MDI magnetogram at 06:27 UT with the outline of the Hα filament absorption feature (at 06:36 UT) overplotted. The orientation and location of the Hα filament agree well with the WNL in the smoothed magnetogram (Fig. 2), with the southern end of the filament rooted above the north-south portion of the WNL and curving eastward above the negative polarity spot. The Hα filament fills only a portion of the filament channel and the underlying magnetic structure extends beyond (Martin 1998).

3. CORONAL DYNAMICS AND EVOLUTION

The coronal structure and dynamics preceding and during the eruption are scrutinized using SECCHI EUVI wavelet-enhanced (Stenborg et al. 2008) anaglyph images and movies in three wavelengths, EUV 171 Å, 195 Å, and 304 Å (see Fig. 1). EUV brightenings are observed to travel eastward along the curved filament material in the 304 Å movie (see Fig. 1 and Liewer et al. 2008). These brightenings intensified during the 2 hours prior to the eruption. A transient, rising, loop-brightening (with a cusp at the apex) on the upper edge of the filament was observed about 1 hour before the eruption in the 171 Å and 195 Å movies, suggesting some preeruption activity near the separator boundary. The bright coronal loops over the CNL (corresponding to the green flux system) build up slowly prior to the filament liftoff, and then much more rapidly during the eruption, indicative of continued flux transfer throughout the eruption process. The flare arcade was brightest at the southern end of the filament material over the WNL (Fig. 4*e*, *blue arrow*). Simultaneous brightenings were seen along the underside of the entire erupting filament (*yellow arrows*) during the erup-

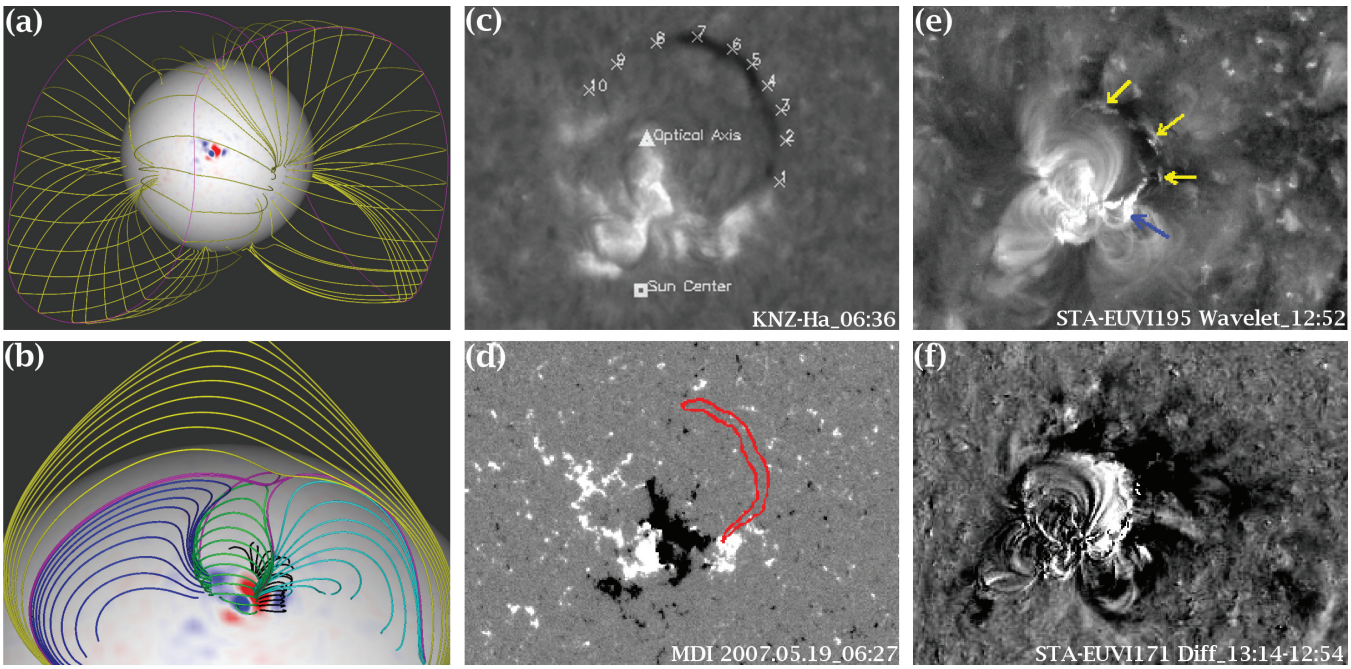

FIG. 4.—(*a*) PFSS model approximation of the global coronal magnetic field structure of 2007 May 19. (*b*) PFSS field lines originating from AR 10956. The black arcade overlies the WNL associated with the filament. Flux systems are color coded as green (CNL arcade), dark blue (ENL arcade), light blue (WNL arcade, overlying black arcade), and yellow (large-scale overlying streamer belt arcade). The purple lines mark topological separation between the flux systems. (*c*) Hα image at 6:36 UT overlaid with tie-points (marked as crosses) of the filament observed in EUVI (*A* and *B*) 304 Å data. (*d*) The outline of the Hα filament overplotted on the magnetogram at 6:27 UT. (*e*) A partial EUVI *A* 195 Å wavelet-enhanced image at 12:52 UT (also see Fig. 1). The arrows point to posteruption bright arcades. (*f*) A contrast-enhanced difference image of the original EUVI *A* 171 Å images (13:14 minus 12:54 UT), showing both the spatial extent of dimming (*dark*) and the central-arcade loops (*bright*).

tion, indicative of the occurrence of reconnection-related heating processes.

Figure 4*f* is a zoomed view of a contrast-enhanced difference image from the *STEREO A* EUVI 171 Å movie where the growth of the central arcade is seen as a bright loop feature. The dark region in Figure 4*f* shows the EUV dimming region, which appears to match the entire extent of the flux system (*light blue*) over the erupting filament. The first sign of the dimming was at 12:52 UT shortly after the flare and the maximum spatial extent of the dimming occurred at 13:12 UT. The coronal dimming was readily observed in EUVI 171 Å and 195 Å images, but much less noticeable in 284 Å. Coronal dimmings, observed simultaneously in multiwavelength EUV emission and soft X-ray images, are one of the classic coronal observables for CMEs (Thompson et al. 1998; Reinard & Biesecker 2008), showing the density depletion associated with the CME eruption and expansion. Coronal dimming may be interpreted as either the footpoints of the CME flux rope (Webb et al. 2000), the larger scale overlying field temporarily opened by the eruption, or some dynamic, evolving combination of the two (e.g., Attrill et al. 2007). A coronal EUV wave is generated by the eruption, initially heading northwest and quickly becoming a full 360° wave front propagating across the EUV disk face (Long et al. 2008). The filament material was in the field of view of 304 Å images for ~3 hr after the liftoff, and showed a significant counterclockwise rotation (see Fig. 1).

4. PROSPECTS FOR MHD MODELING OF CME INITIATION

From the photospheric and coronal magnetic field analysis, taken together with the multiwavelength wavelet-enhanced EUVI movies, we have attempted to relate various aspects of the observations to the initiation process of the 2007 May 19 eruption. We find a variety of features that appear compatible with a number of different CME models, similar to the event examined by Williams et al. (2005). Thus, we cannot specify any one model definitively.

Magnetic breakout.—The most obvious feature in support of the breakout model (Antiochos et al. 1999; Lynch et al. 2008) is the multipolar topology and AR complexity, although this is not sufficient to prove the eruption is solely the result of a breakout process. In the EUVI observations there are also breakout-consistent preeruption features that suggest activity near the separator and possible flux transfer, such as the transient rising loop/cusp above the filament and the slow growth of the CNL flux system.

Tether cutting and flux cancellation.—The eastward-traveling brightenings are seen threading the filament material before the eruption, which supports the tether-cutting (Moore et al. 2001) or flux-cancellation models (Linker et al. 2001; Roussev et al. 2004). However, the fact that the flux cancellation occurred primarily at the CNL and only weakly at the WNL of the filament (§ 2) may better support interpretation as a lateral breakout or a flux-rope-type eruption process. Since it is unclear how much flux cancellation would be required to destabilize the filament, and at least some flux cancellation is observed along the WNL, we cannot exclude either a tether-cutting or flux-cancellation initiation.

Erupting flux rope.—The filament motions during the eruption, best seen in the EUVI 304 Å movie, including helical twisting, writhing, and a large-scale rotation, are most commonly associated with flux rope eruptions (e.g., Green et al. 2007). If the filament channel magnetic structure was a preexisting flux rope, the eruption may be the result of ideal MHD instabilities such as kinking (Török & Kliem 2005) or the torus instability (Kliem & Török 2006). For the kink instability, one would have to show that the flux rope exceeded the critical twist threshold required. The filament spine appears to have a semicircular shape, which could favor the torus instability if this shape was also an accurate representation of the filament's magnetic field structure.

Proponents of the various CME initiation mechanisms discussed above (and others) are encouraged to continue detailed analysis of this unique set of observations. The modelers and theorists are likewise encouraged to demonstrate the ability of their models to reproduce various physical and observational properties of this event.

We acknowledge support from NSF ATM 04-51438, ATM 06-21725, and ATM 01-20950; NASA NNX08AJ04G, NNG06GE51G, and NAS5-03131; and JPL, Caltech. Major data sources are *STEREO*, *SOHO* MDI, BBSO, *Hinode*, and *GOES*.

REFERENCES

Antiochos, S. K., DeVore, C. R., & Klimchuk, J. A. 1999, ApJ, 510, 485
Attrill, G., Harra, L. K., van Driel–Gesztelyi, L., & Démoulin, P. 2007, ApJ, 656, L101
Aulanier, G., DeLuca, E. E., Antiochos, S. K., McMullen, R. A., & Golub, L. 2000, ApJ, 540, 1126
Green, L. M., Kliem, B., Török, T., van Driel–Gesztelyi, L., & Attrill, G. 2007, Sol. Phys., 246, 365
Howard, R. A., & the SECCHI Team. 2007, Space Sci. Rev., in press
Huttunen, K. E. J., et al. 2008, Sol. Phys., submitted
Kliem, B., & Török, T. 2006, Phys. Rev. Lett., 96(25), 255002
Li, Y., & Luhmann, J. G. 2006, ApJ, 648, 732
Liewer, P. C., et al. 2008, Sol. Phys., submitted
Linker, J. A., Lionello, R., Mikić, Z., & Amari, T. 2001, J. Geophys. Res., 106(A11), 25165
Long, D.M., Gallagher, P.T., McAteer, R.T.J., and Bloomfield, D.S. 2008, ApJ, 680, L81
Luhmann, J. G., Gosling, J. T., Hoeksema, J. T., & Zhao, X. 1998, J. Geophys. Res., 103(A4), 6585
Lynch, B. J., Antiochos, S. K., DeVore, C. R., Luhmann, J. G., & Zurbuchen, T. H. 2008, ApJ, in press
Martin, S. F. 1998, Sol. Phys., 182, 107
Moore, R. L., Sterling, A. C., Hudson, H., & Lemen, J. R. 2001, ApJ, 552, 833
Reinard, A. A., & Biesecker, D. A. 2008, ApJ, 674, 576
Roussev, I. I., Sokolov, I. V., Forbes, T. F., Gombosi, T. I., Lee, M. A., & Sakai, J. I. 2004, ApJ, 605, L73
Scherrer, P. H., et al. 1995, Sol. Phys., 162, 129
Stenborg, G., Vourlidas, A., & Howard, R. A. 2008, ApJ, 674, 1201
Thompson, B. J., Plunkett, S. P., Gurman, J. B., Newmark, J. S., St. Cyr, O. C., & Michels, D. J. 1998, Geophys. Res. Lett., 25(14), 2465
Török, T., & Kliem, B. 2005, ApJ, 630, L97
Webb, D. F., et al. 2000, J. Geophys. Res., 105(A12), 27251
Welsch, B. T. 2006, ApJ, 638, 1101
Williams, D. R., Török, T., Démoulin, P., van Driel–Gesztelyi, L., & Kliem, B. 2005, ApJ, 628, L163
Wulser, J.-P., & the EUVI Team. 2004, Proc. SPIE, 5171, 111